OPEN

NPG Asia Materials (2015) 7, e190; doi:10.1038/am.2015.57

www.nature.com/am

ORIGINAL ARTICLE

Novel high-κ dielectrics for next-generation electronic devices screened by automated *ab initio* calculations

Kanghoon Yim[1,2], Youn Yong[1,2], Joohee Lee[1,2], Kyuhyun Lee[1,2], Ho-Hyun Nahm[3,4], Jiho Yoo[5], Chanhee Lee[5], Cheol Seong Hwang[1,2] and Seungwu Han[1,2]

As the scale of transistors and capacitors in electronics is reduced to less than a few nanometers, leakage currents pose a serious problem to the device's reliability. To overcome this dilemma, high-κ materials that exhibit a larger permittivity and band gap are introduced as gate dielectrics to enhance both the capacitance and block leakage simultaneously. Currently, HfO_2 is widely used as a high-κ dielectric; however, a higher-κ material remains desired for further enhancement. To find new high-κ materials, we conduct a high-throughput *ab initio* calculation for band gap and permittivity. The accurate and efficient calculation is enabled by newly developed automation codes that fully automate a series of delicate methods in a highly optimized manner. We can, thus, calculate >1800 structures of binary and ternary oxides from the Inorganic Crystal Structure Database and obtain a total property map. We confirm that the inverse correlation relationship between the band gap and permittivity is roughly valid for most oxides. However, new candidate materials exhibit interesting properties, such as large permittivity, despite their large band gaps. Analyzing these materials, we discuss the origin of large κ values and suggest design rules to find new high-κ materials that have not yet been discovered.
NPG Asia Materials (2015) **7,** e190; doi:10.1038/am.2015.57; published online 12 June 2015

INTRODUCTION

The dielectric insulator is a key component in microelectronic devices such as the central processing unit (CPU), dynamic random-access memory (DRAM) and flash memory. The basic function of the dielectric material is to enhance the capacitive coupling between adjacent metals and semiconductors, although it should also suppress the leakage current between electrodes, which undermines the energy consumption (in CPU and DRAM) or long-term reliability (in flash memory). In past decades, silicon dioxide (SiO_2) has been used as an archetypical dielectric material because it allows for defect-free, high-quality thin-film growth. As the integration level of microelectronic devices is currently exponentially increasing, the thickness of SiO_2 has decreased to maintain the device performance. However, if the SiO_2 layer becomes thinner than ~1 nm, the leakage current due to the quantum tunneling effect begins to dominate,[1] which causes serious problems in power consumption and device performance. This technical obstacle has been overcome by replacing SiO_2 with insulators that possess high dielectric constants (high-κ).[1,2] With high-κ dielectrics, the dielectric thickness can be increased at the same capacitance, thereby suppressing the leakage current.[3] Currently, the favored high-κ dielectrics are HfO_2 (as the gate dielectric in CPU),[2] ZrO_2 (as the capacitor dielectric in DRAM)[4] and Al_2O_3 (as the blocking oxide in charge-trap flash memory).[3]

In addition to a large dielectric constant, the high-κ dielectric is required to have a large band gap (E_g) to suppress the charge injection from electrodes into dielectrics that cause the leakage current. Therefore, the ideal high-κ dielectrics should possess both large E_g and κ. Notably, when E_g and κ of well-known oxides are plotted (see Figure 1), the trade-off relation is clearly noticeable. That is, materials are abundant with large E_g (> ~8 eV) or high κ (> ~20); however, no material has been discovered that satisfies both conditions simultaneously. Because this observation is based on a limited set of materials, one may question whether a material possessing both large E_g and κ may indeed exist if the search space is expanded.

Obtaining material information on E_g and κ, particularly the static dielectric constant, would be prohibitive if only experimental measurements were utilized. However, with the recent advances in computational methods and facilities, it is now feasible to compute *ab initio* various physical properties of the bulk phase in a relatively short period. Recently, several attempts have been made to find an optimal functional material using high-throughput computational screening.[5–8] The machine-learning approach presented by G. Pilania[9] is a more accelerated approach to predict properties of large numbers of polymers; however, the prediction accuracy for E_g and κ is low for extending the method to other systems. In this study, we perform *ab initio* calculations on ~1800 oxides (except for 3*d* transition metal oxides) that cover most binary and ternary oxides

[1]Department of Materials Science and Engineering, Seoul National University, Seoul, South Korea; [2]Research Institute of Advanced Materials, Seoul National University, Seoul, South Korea; [3]Center for Correlated Electron Systems, Institute for Basic Science (IBS), Seoul, South Korea; [4]Department of Physics and Astronomy, Seoul National University, Seoul, South Korea and [5]Platform Technology Lab., SAIT, Samsung Materials Research Complex, Yeong Tong-gu, Gyeonggi-do, South Korea
Correspondence: Professor S Han, Department of Materials Science and Engineering, Seoul National University, 30-422, 1 Gwanak-ro, Gwanak-gu, Seoul 151-744, South Korea.
E-mail: hansw@snu.ac.kr
Received 15 November 2014; revised 24 February 2015; accepted 14 April 2015

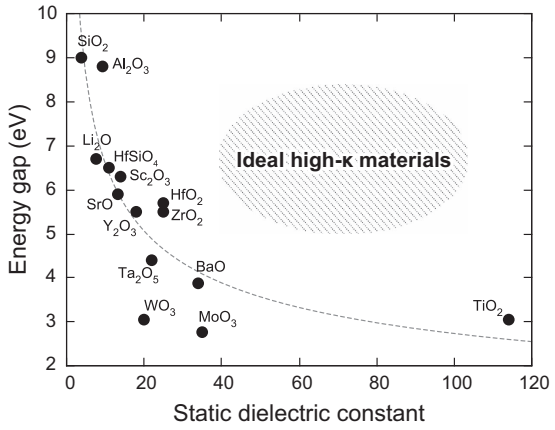

Figure 1 The experimental band gap and dielectric constant for well-known oxides. The property region ideal for dielectrics is also shown.

identified to date and suggest novel candidate high-κ dielectrics suitable for each device type. To this end, we set up computational machinery that automatically fetches structures from the database, prepares input files and reliably performs the *ab initio* calculations.

MATERIALS AND METHODS

Figure 2 presents a brief scheme of our automation strategy for calculating E_g and κ. First, all of the structures that contain specific cations are collected from the Inorganic Crystal Structure Database.[10] We exclude 3*d* transition metal atoms because the electronic correlation effects are strong and E_g is moderate (<3 eV). The structures are further screened to avoid duplicative calculations on the same structure. The structures with partial atomic occupation are excluded because of the difficulty in computational modeling. In addition to the structures that are stable at ambient conditions, we consider structures that are characterized under high-temperature or high-pressure conditions, provided that they are theoretically stable at zero temperature and pressure conditions, because the metastable structures can exist at ambient conditions through doping[11] or in nanocrystalline states.[12] The atomic positions and lattice parameters are then relaxed, and the theoretical equilibrium structures are obtained. For the computational code, the Vienna *Ab Initio* Simulation Package[13] is adopted as the core engine for the *ab initio* calculations. Regarding the exchange-correlation functional between electrons, we employ the generalized gradient approximation (GGA)[14] for E_g and local density approximation (LDA)[15] for κ. Because GGA and LDA underestimate the band gap, we also perform a hybrid-functional calculation for the band-edge points identified by GGA. The detailed procedure for each step is provided in the Methods section. The reliability of the present automation procedure is confirmed by comparing the extant experimental data with previous calculations.

Structural relaxation

All experimental structures should first be relaxed theoretically. This step is mandatory because when computing a dielectric constant, the structures are assumed to be at the local equilibrium. The **k**-points in the first Brillouin zone are carefully and automatically sampled such that the total energy and stress tensor components are converged within 5 meV per atom and 10 kbar, respectively. The energy cutoff for the plane-wave basis set is selected based on the atomic species and pseudopotential types. The structural relaxation is performed until the atomic force and stress tensor are reduced to below 0.02 eV Å^{-1} and 5 kbar, respectively. Many structures reported at high-temperature or high-pressure conditions often have higher symmetry compared with low-temperature phases. When these structures are relaxed with the symmetry maintained, the final structures often possess unstable phonon modes. We exclude these structures from consideration as new high-κ candidates because of their stability issue.

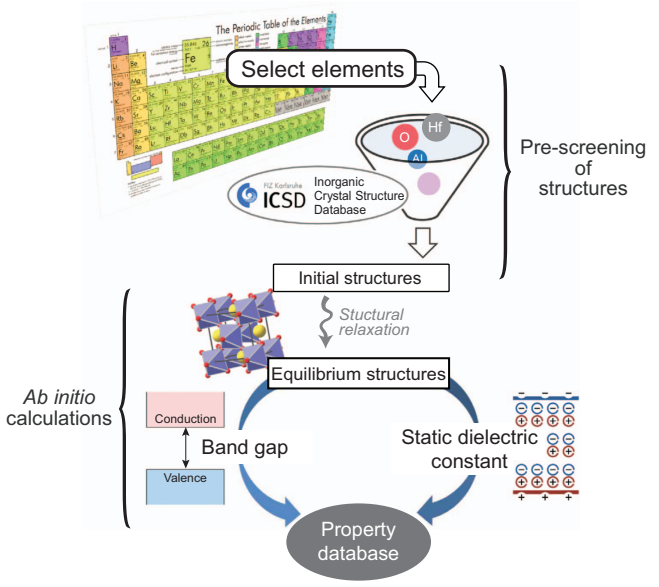

Figure 2 Schematic automation strategy to collect computational data on the band gap and static dielectric constant. The initial structures collected from the ICSD were filtered for the ensuing *ab initio* computations.

Computation of band gap

We first computed energy levels along the lines connecting the high-symmetry **k**-points within GGA.[16] On the basis of the results, the **k**-points corresponding to the valence top and conduction minimum are determined. Because the band gap underestimation is severe in the semilocal functional, we additionally perform a hybrid-functional (HSE06) calculation[17] (without further structural relaxation) and calculate the energy levels at the band-edge **k**-points identified by GGA (this scheme is called HSE@GGA hereafter). This process assumes that the band structure rigidly shifts upon application of the hybrid functional. Supplementary Figure S1 in the Supplementary Information shows that the band structure from the hybrid functional is approximately a rigid shift of the GGA result. By adopting the HSE@GGA scheme, we could significantly reduce the computational cost compared with the full hybrid-functional calculations. For oxides that include heavy elements such as Tl, Pb and Bi, the spin-orbit coupling is included in computing E_g.

To ensure the reliability of the present scheme, test calculations on several oxides are performed and compared with the experiment and previous GGA calculations (see Figure 3a). The estimated energy gaps are in good agreement with the experiment, although sizeable errors of up to 1 eV are noticeable for oxides with E_g larger than ~4 eV. These errors are due to the fixed fraction of the exact exchange term in the HSE06 functional, which should be increased in the large-gap materials.[18] This finding implies that more sophisticated methods such as GW calculations can be utilized to obtain more precise values of E_g. We note that the GW calculations are too expensive to be incorporated into the high-throughput screening. In addition, it is not yet known which level of GW approximations can be universally applied to every class of oxides.[19] Nevertheless, the accuracy of HSE@GGA is sufficient to screen promising dielectrics in the present study.

Computation of dielectric constant

To compute the electronic permittivity, the linear-response method based on the density functional perturbation theory is used to obtain Born effective charges and phonon modes at the zone center.[20] Because the linear-response computation is sensitive to the **k**-point sampling, we double the **k**-point density along each direction. The static dielectric constant ($\varepsilon^0_{\alpha\beta}$) is then calculated using the following formula:

$$\varepsilon^0_{\alpha\beta} = \varepsilon^{\infty}_{\alpha\beta} + \frac{4\pi}{\Omega}\sum_m \frac{Z^*_{m\alpha}Z^*_{m\beta}}{\omega^2_m}, \quad (1)$$

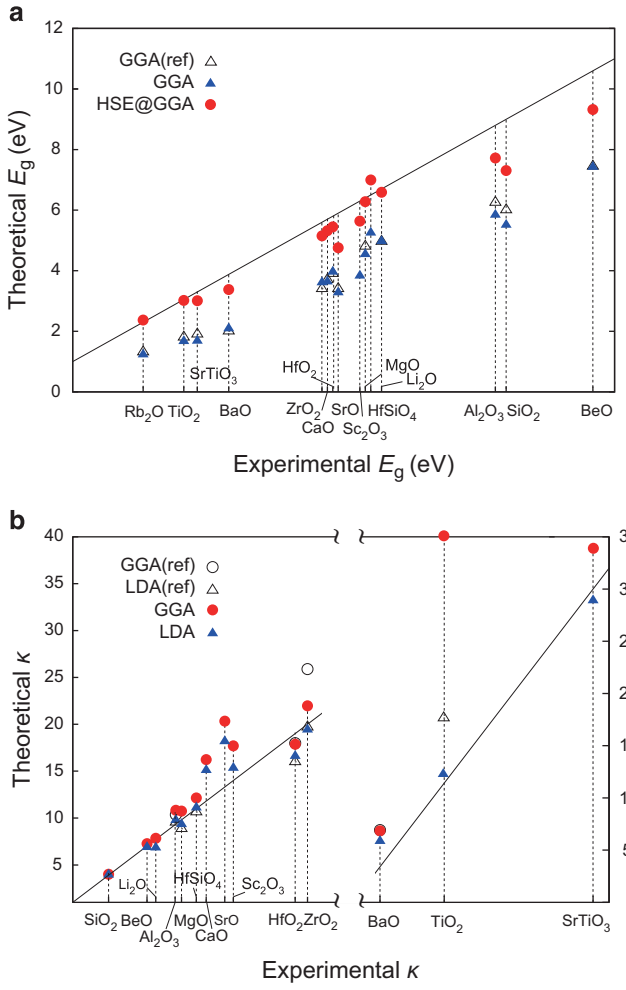

Figure 3 Comparison of theoretical and experimental data for the (**a**) band gap (E_g) and (**b**) static dielectric constant (κ); some reference data from other *ab initio* studies (LDA(ref) and GGA(ref)) are also shown as open symbols.[20,33–39] The solid line indicates perfect agreement with the experiment. HSE@GGA indicates the band gap obtained using the hybrid-functional calculations on the band-edge points identified by GGA.

where $\varepsilon^0_{\alpha\beta}$, Ω, ω_m and Z^*_m denote the dielectric tensor contributed by electrons, the unit-cell volume, the frequency of the infrared-active phonon with the mode number of m and the mode-effective Born effective charges, respectively. The subscripts α and β in equation (1) indicate the directions. The dielectric constant (κ) is obtained by averaging the diagonal components of $\varepsilon^0_{\alpha\beta}$. The theoretical κ of some oxides determined by GGA and LDA are compared with the experiment (see Figure 3b). The mean absolute errors for materials with $\kappa < 30$ are 2.06 and 1.37 for the GGA and LDA results, respectively. The GGA results exhibit larger errors than those of LDA because the ionic part of κ is sensitive to the low-frequency phonon modes that are significantly softened when the lattice parameters are expanded in GGA. Therefore, we employ LDA for computing κ.

Computational cost

The average computational cost was ~70 CPU hours per structure on the 24-core cluster. The most time-consuming part was the hybrid-functional calculation in the HSE@GGA scheme (50%) followed by the density functional perturbation theory calculations for the dielectric constant (27%). The structure relaxation and band-edge searching consumed ~15% and 8% of the total computational time, respectively.

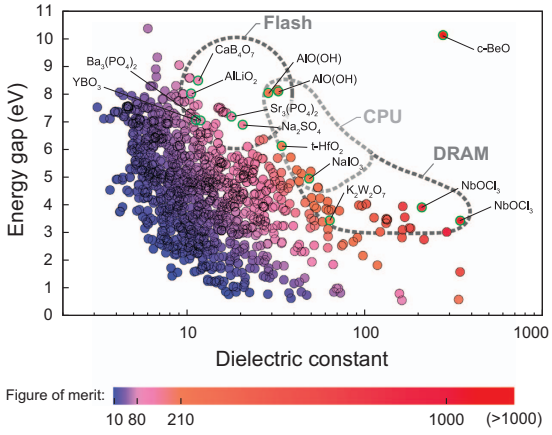

Figure 4 E_g vs κ plot for computed structures for 1158 oxides. Each point is color coded according to the figure of merit (E_g·κ). The candidate oxides that have not yet been tested are indicated by the chemical formula. The rough boundary of material properties that are adequate for each device type is marked by dashed lines. CPU, central processing unit.

RESULTS

Total property map

We calculated 1762 oxides in total and obtained a large property database. Figure 4 presents the property map of E_g versus κ for 1158 binary and ternary oxides. We excluded the structures that were metallic or unstable under the ambient condition according to the results. First, the inverse relation between E_g and κ was roughly valid, and the oxides satisfying the ideal condition were scarce. To select candidate high-κ oxides from the database, we defined a figure of merit for reducing the leakage current. The leakage current density by direct tunneling (J_{DT}) can be expressed using the following semi-empirical formula:[21]

$$J_{DT} \propto exp\left\{-\frac{2\sqrt{2|q|}}{\hbar}\cdot\left(m_{eff}\Phi_b\right)^{1/2}\kappa\cdot t_{ox,eq}\right\}, \quad (2)$$

where q and m_{eff} are the charge and tunneling effective mass, respectively, of the electron or hole, Φ_b is the injection barrier, and $t_{\text{ox,eq}}$ represents the equivalent oxide thickness. We define $(m_{\text{eff}}\ \Phi_b)^{1/2}\kappa$ in the exponent as the figure of merit (f_{FOM}), which indicated that the tunneling current is exponentially suppressed with f_{FOM}. One can compute m_{eff} and Φ_b theoretically,[22] but the process requires demanding calculations that are not compatible with the high-throughput approach. Here we make a crude but reasonable assumption that the two parameters are roughly proportional to E_g,[23] which approximates f_{FOM} as simply E_g·κ. Each point in Figure 4 is color coded according to f_{FOM}.

New candidate high-κ materials

Among the oxides in Figure 4, c-BeO, the high-pressure phase of BeO in the rocksalt structure (see Figure 5a), is particularly prominent as it has the unusual combination of 10.1 eV and 275 for E_g and κ, respectively. Consequently, its f_{FOM} is considerably beyond those of other materials. The wurtzite BeO (w-BeO), which is stable at ambient conditions, has already been used in dielectric applications as it has the largest band gap among all the oxides. The atomic-layer-deposited w-BeO was fabricated on Si substrates and employed as a diffusion barrier of oxygen between Si and high-κ dielectrics such as HfO_2.[24] However, w-BeO has a very small κ of ~7. However, c-BeO has not

been applied in microelectronic devices to date as far as we are aware. The origin of the large κ of c-BeO is its soft optical phonon mode (~3.5 THz), wherein the Be and O atoms vibrate in opposite directions (see Figures 5a and b). In c-BeO, the Be–O bond length is longer than that in w-BeO by 0.11 Å, which softens the optical phonon mode. The computed total energy indicates that c-BeO is less stable than w-BeO by 0.483 eV per atom. The large energy difference implies that c-BeO would be difficult to stabilize under ambient conditions. However, we pay attention to the experiments in Adelmann *et al.*[25], Kita *et al.*[26] and Tsipas *et al.*[27], which indicate that the high-temperature phases of HfO_2 and ZrO_2 can be synthesized as thin films by external doping or strain. More importantly, the doped phases possessed increased dielectric constants, as predicted by theory.[28] Therefore, we reasonably expect that c-BeO can be stabilized by doping or strain and will exhibit physical properties similar to the present calculations.

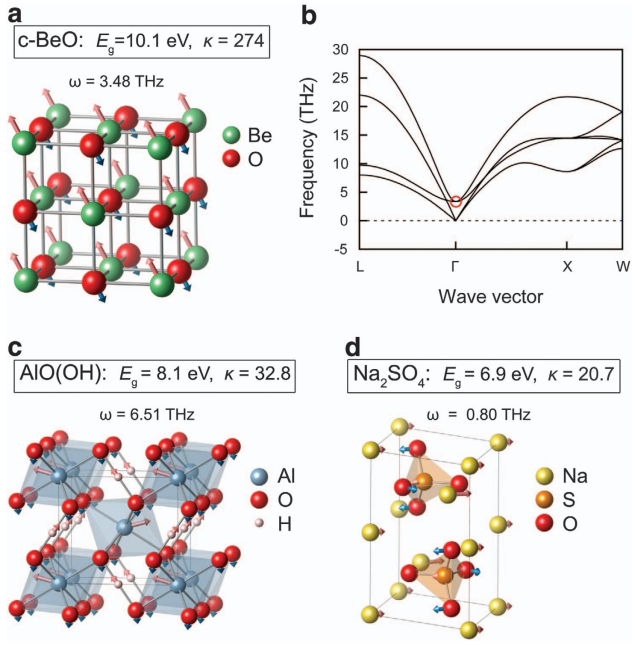

Figure 5 (**a**) The unit-cell structure of c-BeO and the lowest phonon mode indicated by arrows. The frequency of this mode (ω) is also noted. (**b**) The phonon dispersion curve of c-BeO. The lowest phonon mode (threefold degenerate) is marked by a circle. The unit-cell structure of (**c**) $NbOCl_3$ and (**d**) Na_2SO_4. The lowest phonon modes that are responsible for most of κ are shown in each structure with the vibrational directions indicated by arrows.

Except for c-BeO, we could not find any outstanding high-κ dielectrics with either E_g or κ larger than those of the HfO_2 thin films currently used in CPU or DRAM ($E_g \sim 6.0$ eV and $\kappa \sim 20$–25; see t-HfO_2 in Figure 4). Nevertheless, we identified several candidates that are noteworthy and list them in Table 1. These materials could be important in the future as the main material shifts from Si to Ge and GaAs and a more diverse selection of gate dielectrics is highly demanded to meet chemical conditions that are different from Si. Here we exclude oxides that have been studied previously. In the last column of Table 1, we mark the appropriate device type according to the material properties; for CPU and DRAM devices, the international technology roadmap of semiconductors states that further device scaling requires higher-κ dielectrics with $\kappa > 30$.[29] We note the candidate high-κ materials that satisfy this condition and have larger f_{FOM} than that of t-HfO_2 ($f_{FOM} \sim 210$). We also limited $E_g > 4$ eV for CPU and $E_g > 3$ eV for DRAM, considering that the ideal Φ_b should be at least > 1.5 eV. For the blocking oxides used in flash memory, large values of E_g are more crucial than large κ to satisfy the more stringent leakage current specification ($< \sim 10^{-9}$ Acm^{-2}) compared with DRAM ($< \sim 10^{-7}$ Acm^{-2}) and CPU ($< \sim 10^{-1}$ Acm^{-2}). We, therefore, impose the condition of $E_g > 6$ eV and $f_{FOM} > 80$, which is larger than the values for Al_2O_3, the currently favored high-κ blocking oxide in the charge-trap flash memory. The total candidate lists including those for DRAM and Flash are provided in Tables 2 and 3, respectively. For the gate dielectric for CPU, we further consider that the stability of high-κ/Si interfaces is important to prevent the unintentional oxidation of the Si substrate. One metric of oxide stability is the formation energy of oxygen vacancies (E_{vac}) because it reflects the strength of metal–oxygen bonding. The computed E_{vac}s for the candidate materials are listed in Table 1. Because the E_{vac} of SiO_2 is 5.6 eV, oxides with E_{vac} values larger than this value may form a stable interface with Si. For example, it is known that ZrO_2 ($E_{vac} = 5.1$ eV) exhibits a stability issue on Si substrates,[30] whereas HfO_2 ($E_{vac} = 6.9$ eV) is stable. This behavior is reflected in selecting candidate oxides for CPU in Table 1. ΔE per atom in Table 1 denotes the total energy

Table 1 New candidate materials suitable for high-κ dielectrics selected from Figure 3

Name	*ICSD*	*κ*	E_g *(eV)*	f_{FOM}	*ΔE per atom (eV)*	E_{vac}*(eV)*	*CPU*	*DRAM*	*Flash*
c-BeO	163825	274.8	10.11	2780	0.483	6.62	✓	✓	✓
$NbOCl_3$	26471	343.4	3.43	1176	0.002	4.91		✓	
$NbOCl_3$	412071	208.8	3.90	815	0	4.81		✓	
δ-AlO(OH)	166337	32.78	8.09	265	0.031	4.65		✓	✓
$NaIO_3$	202679	48.84	4.94	241	0	2.11		✓	
δ-AlO(OH)	166331	28.82	8.03	231	0.026	7.08	✓	✓	✓
$K_2W_2O_7$	67284	63.70	3.43	219	0	3.93		✓	
Na_2SO_4	66554	20.70	6.89	143	0.004	3.24			✓
$Sr_3(PO_4)_2$	30635	17.90	7.18	129	0	5.06			✓
CaB_4O_7	412710	11.64	8.48	99	0	6.25			✓
$AlLiO_2$	28288	10.64	8.01	85	0.024	7.05			✓
$Ba_3(PO_4)_2$	30634	12.02	7.03	85	0	5.06			✓
YBO_3	100015	11.33	7.05	80	0	6.22			✓

Abbreviation: ICSD, Inorganic Crystal Structure Database.
ΔE per atom is the relative energy with respect to theoretically the most stable structure. E_{vac} is the formation energy of neutral oxygen vacancy. The suitable application for each material is marked in the last three columns.

Table 2 All high-κ candidate materials for DRAM and CPU from the present property database, which satisfy $f_{FOM} > 210$, and $E_g > 3$ eV (for DRAM) or $E_g > 4$ eV (for CPU)

Name	*ICSD*	*Space group*	*κ*	E_g *(Ev)*	f_{FOM}
BeO	163825	225	274.80	10.11	2780
$NbOCl_3$	26471	136	343.40	3.43	1176
$SrTiO_3$	201256	221	288.12	3.01	869
$NbOCl_3$	412071	113	208.83	3.90	815
$NaNbO_3$	247316	33	163.36	3.94	643
$NaTaO_3$	88377	127	167.76	3.55	595
$AgTaO_3$	40830	161	180.95	3.15	570
$AgTaO_3$	40831	167	177.85	3.16	563
$SrTiO_3$	182762	140	162.94	3.09	504
Li_4CO_4	245400	8	62.39	7.83	489
$CdTiO_3$	62150	62	134.28	3.45	464
$CdTiO_3$	51698	26	132.24	3.50	462
$CdTiO_3$	262711	33	133.47	3.46	461
$KTaO_3$	56440	221	131.87	3.33	439
$Y_2Ti_2O_7$	15633	227	101.98	4.02	410
$Cd_2Ta_2O_7$	75605	227	112.80	3.53	399
$NaTaO_3$	88375	62	96.60	3.96	382
TiO_2	202241	136	122.10	3.02	369
$NaTaO_3$	980	62	92.71	3.98	369
$PbHfO_3$	89326	55	72.14	3.78	273
AlO(OH)	166337	58	32.78	8.09	265
AlO(OH)	166345	58	32.42	8.14	264
$SrHfO_3$	161595	127	49.92	5.19	259
$Ag_2Ta_4O_{11}$	180734	167	61.83	4.11	254
$BaZrO_3$	43136	221	54.57	4.62	252
$PbZrO_3$	31154	32	65.13	3.82	249
$NaIO_3$	202679	62	48.84	4.94	241
$BiTaO_4$	97423	52	56.17	4.23	238
$PbHfO_3$	174106	55	62.69	3.79	238
$PbHfO_3$	33194	32	60.85	3.84	234
AlO(OH)	166331	31	28.82	8.03	231
$HfTe_3O_8$	9078	206	44.14	5.12	226
ZrO_2	93031	137	38.53	5.71	220
$K_2W_2O_7$	67284	14	63.70	3.43	219
$Sr_2Ta_2O_7$	16388	36	50.30	4.25	214

Abbreviations: CPU, central processing unit; ICSD, Inorganic Crystal Structure Database.

Table 3 All high-κ candidate materials for flash memory application from the present property database, which satisfy $f_{FOM} > 80$ and $E_g > 6$ eV

Name	*ICSD*	*Space group*	*κ*	E_g *(eV)*	f_{FOM}
BeO	163825	225	275	10.11	2780
AlO(OH)	166345	58	32.4	8.14	264
AlO(OH)	166331	31	28.8	8.03	231
HfO_2	173966	137	34.3	6.12	210
$LaYO_3$	419666	62	25.8	6.32	163
Na_2SO_4	66554	63	20.7	6.89	143
$Sr_3(PO_4)_2$	30635	166	17.9	7.18	129
$YAlO_3$	4115	62	16.1	7.36	119
$MgSiO_3$	171911	62	15.5	7.49	116
YOCl	60586	129	15.2	6.53	99
CaB_4O_7	412710	31	11.6	8.48	99
$MgAl_2O_4$	157186	62	14.2	6.80	96
Ba_2SiO_4	28476	62	15.0	6.21	93
B_2O_3	51575	152	10.5	8.57	90
$Mg_4O_3(OH)_2$	95470	164	14.2	6.28	89
$Ba_3P_4O_{13}$	280908	2	13.0	6.85	89
B_2O_3	36066	144	10.4	8.57	89
Li_3OBr	67265	221	11.6	7.61	88
$Mg(OH)_2$	79031	164	13.4	6.59	88
$MgSiO_3$	172736	63	13.1	6.57	86
$Y_2(Si_2O_7)$	164148	2	13.3	6.41	85
$AlLiO_2$	28288	166	10.6	8.01	85
YOF	76426	129	12.9	6.57	85
$Ba_3(PO_4)_2$	30634	166	12.0	7.03	85
SrB_4O_7	95300	31	9.12	9.03	82
$BaSO_4$	33730	62	10.4	7.79	81

Abbreviation: ICSD, Inorganic Crystal Structure Database.

per atom relative to the most stable phase identified from the present computation and indicates the relative thermal stability of the given phase.

DISCUSSION

In Figures 5c and d, the structures of two candidate oxides, AlO(OH) and Na_2SO_4, are displayed together with the lowest phonon mode, indicated by arrows. These structures exhibit the two representative features of high-κ ternary oxides. In the lowest phonon modes of AlO(OH) (Figure 5c), cations vibrate within the octahedral cage formed by anions. In contrast to face-sharing octahedra in Al_2O_3, H^+ ions in AlO(OH) lead to corner sharing, which softens the vibrational mode of Al^{3+}. $NbOCl_3$ in Table 1 also has a similar feature of cationic vibration within the corner-sharing octahedra. However, all of the other ternary oxides in Table 1 have another common feature, which can be represented by Na_2SO_4 in Figure 5d: they usually contain non-metal oxygen units such as $(SO_4)^{2-}$, $(PO_4)^{3-}$ and $(IO_3)^-$. These units form a rigid bond in the compounds, whereas the other type of cation is loosely bound to oxygen and yields soft phonon modes (see Na atoms in Figure 5d). Furthermore, we find that the unblocked cation channel is critical for a large dielectric constant. For example, two polymorphs of Na_2SO_4 have common orthorhombic phases but slightly different atomic arrangements with a crystal symmetry of *Cmcm* and *Pbnm*, respectively (see Supplementary Figure S2 in Supplementary Information). The coordination number and oxidation state of each atom are similar, and E_g is thus almost the same. However, the two κ values significantly differ (*Cmcm*: 20.7 vs *Pbnm*: 5.9).

For the *Cmcm* structure, as shown in Figure 5d, all of the cations in the soft mode vibrate coherently along certain passages without being blocked by other species of atoms. However, such an unblocked channel does not exist in the *Pbnm* phase. Consequently, the Na atoms oscillate in rather random directions, and the contributions to dielectric polarization cancel each other out, resulting in smaller κ. Note that the ionic conduction of Na^+ can cause device instability[31]. However, considering the lower ionic conductivity in the *Cmcm* structure compared with that for other phases[32], we cautiously believe that the high-κ phase of Na_2SO_4 could be employed in microelectronic devices.

On the basis of these observations, high-κ ternary oxides that simultaneously exhibit large E_g and κ might be identified through two models: (1) cationic vibration within the corner-sharing octahedral cage of anions and (2) channeled structures formed by a combination of metal ions and various non-metal oxide units. Considering the numerous possible combinations to form ternary oxides, we expect that several ideal dielectric materials that have these features could be identified in the future.

In summary, we screened ~1800 binary and ternary oxides using high-throughput *ab initio* calculations of the band gap and static dielectric constant with the aim to find new candidate high-κ dielectrics that can be used in various microelectronic devices such as CPU, DRAM and flash memory. From the obtained property database, we generated a materials map of the band gap versus static dielectric constant and identified new candidate materials that have not been considered in previous studies. From the detailed analysis on the atomic structure and phonon mode, we identified key factors that correlate with the large dielectric constant. By suggesting new candidate high-κ materials and developing a large material property database covering most binary and ternary oxides, the present work will contribute greatly to selecting functional oxides that are optimal for specific applications. An automated high-throughput study on oxygen vacancy defects in oxides is also in progress.

CONFLICT OF INTEREST

The authors declare no conflict of interest.

ACKNOWLEDGEMENTS

This research was supported by the EDISON program (NRF-2012M3C1A6035307). The computations were performed at the KISTI supercomputing center (KSC-2014-C3-012).

1 Kingon, A. I., Maria, J.-P. & Streiffer, S. K. Alternative dielectrics to silicon dioxide for memory and logic devices. *Nature* **406**, 1032–1038 (2000).
2 Robertson, J. High dielectric constant gate oxides for metal oxide Si transistors. *Rep. Prog. Phys.* **69**, 327–396 (2006).
3 Lee, C.-H., Hur, S.-H., Shin, Y.-C., Choi, J.-H., Park, D.-G. & Kim, K. Charge-trapping device structure of SiO_2 /SiN/high-k dielectric Al_2O_3 for high-density flash memory. *Appl. Phys. Lett.* **86**, 152908 (2005).
4 Kim, S. K., Lee, S. W., Han, J. H., Lee, B., Han, S. & Hwang, C. S. Capacitors with an equivalent oxide thickness of <0.5 nm for nanoscale electronic semiconductor memory. *Adv. Funct. Mater.* **20**, 2989–3003 (2010).
5 Hautier, G., Miglio, A., Ceder, G., Rignanese, G.-M. & Gonze, X. Identification and design principles of low hole effective mass p-type transparent conducting oxides. *Nat. Commun.* **4**, 2292 (2013).
6 Fujimura, K., Seko, A., Koyama, Y., Kuwabara, A., Kishida, I., Shitara, K., Fisher, C. A. J., Moriwake, H. & Tanaka, I. Accelerated materials design of lithium superionic conductors based on first-principles calculations and machine learning algorithms. *Adv. Energy Mater* **3**: 8 980–985 (2013).
7 Bennett, J. W. & Rabe, K. M. Integration of first-principles methods and crystallographic database searches for new ferroelectrics: Strategies and explorations. *J. Solid State Chem.* **195**, 21–31 (2012).
8 Curtarolo, S., Hart, Gus, L. W., Nardelli, M. B., Mingo, N., Sanvito, S. & Levy, O. The high-throughput highway to computational materials design. *Nat. Mater.* **12**, 191–201 (2013).
9 Pilania, G., Wang, C., Jiang, X., Rajasekaran, S. & Ramprasad, R. Accelerating materials property predictions using machine learning. *Sci. Rep.* **3**, 2810 (2013).
10 Karlsruhe, F. I. Z. Inorganic Crytal Structure Database, Available at http://icsd.fiz-karlsruhe.de.
11 Lee, C.-K., Cho, E., Lee, H.-S., Hwang, C. S. & Han, S. First-principles study on doping and phase stability of HfO_2. *Phys. Rev. B* **78**, 012102 (2008).
12 McHale, J. M., Auroux, A., Perrotta, A. J. & Navrotsky, A. Surface energies and thermodynamic phase stability in nanocrystalline aluminas. *Science* **277**, 788 (1997).
13 Kresse, G. & Hafner, J. Ab initio molecular dynamics for liquid metals. *Phys. Rev. B* **47**, 558 (1993).
14 Perdew, J. P., Burke, K. & Ernzerhof, M. Generalized gradient approximation made simple. *Phys. Rev. Lett.* **78**, 1396 (1997).
15 Ceperley, D. M. & Alder, B. J. Ground state of the electron gas by a stochastic method. *Phys. Rev. Lett.* **45**, 566 (1980).
16 Setyawan, W. & Curtarolo, S. High-throughput electronic band structure calculations: Challenges and tools. *Comput. Mater. Sci.* **49**, 299 (2010).
17 Heyd, J., Scuseria, G. E. & Ernzerhof, M. J. Hybrid functionals based on a screened Coulomb potential. *Chem. Phys.* **118**, 8207–8215 (2003).
18 Marques, M. A. L., Vidal, J., Oliveira, M. J. T., Reining, L. & Botti, S. Density-based mixing parameter for hybrid functionals. *Phys. Rev. B* **83**, 035119 (2011).
19 Kang, Y., Kang, G., Nahm, H.-H., Cho, S.-H., Park, Y. S. & Han, S. GW calculations on post-transition-metal oxides. *Phys. Rev. B* **89**, 165130 (2014).
20 Lee, C.-K., Cho, E., Lee, H., Seol, K. & Han, S. Comparative study of electronic structures and dielectric properties of alumina polymorphs by first-principles methods. *Phys. Rev. B* **76**, 245110 (2007).
21 Yeo, Y.-C. MOSFET gate leakage modeling and selection guide for alternative gate dielectrics based on leakage considerations. *IEEE Trans. Electron Dev.* **50**: 4 1027 (2003).
22 Robertson, J. Band offsets of wide-band-gap oxides and implications for future electronic devices. *J. Vac. Sci. Technol. B* **18**, 1785 (2000).
23 Hinkle, C.L., Fulton, C., Nemanich, R.J. & Lucovsky, G. A novel approach for determining the effective tunneling mass of electrons in HfO_2 and other high-K alternative gate dielectrics for advanced CMOS devices. *Microelectron. Eng.* **72**, 257–262 (2004).
24 Yum, J. H., Bersuker, G., Akyol, T., Ferrer, D.A., Lei, M., Park, K. W., Hudnall, T. W., Downer, M. C., Bielawski, C. W., Yu, E. T., Price, J., Lee, J. C. & Banerjee, S. K. Epitaxial ALD BeO: efficient oxygen diffusion barrier for EOT scaling and reliability improvement. *IEEE Trans. Electron Dev.* **58**, 4384–4392 (2011).
25 Adelmann, C., Tielens, H., Dewulf, D., Hardy, A., Pierreux, D., Swerts, J., Rosseel, E. X., Shi, E., Van Bael, M. K., Kittl, J.A. & Van Elshochta, S. Atomic Layer Deposition of Gd-Doped Hf02 Thin Films. *J. Electrochem. Soc* **157**, 4 (2010).
26 Kita, K., Kyuno, K. & Toriumi Akira. Permittivity increase of yttrium-doped HfO_2 through structural phase transformation. *Appl. Phys. Lett.* **86**, 102906 (2005).
27 Tsipas, P., Volkis, S. N., Sotiropoulos, A., Galata, S. F., Mavrou, G., Tsoutsou, D., Panayiotatos, Y., Dimoulas, A., Marchiori, C. & Fompeyrine, J. Germanium-induced stabilization of a very high-k zirconia phase in ZrO_2/GeO_2 gate stacks. *Appl. Phys. Lett.* **93**, 082904 (2008).
28 Zhao, X. & Vanderbilt, D. First-principles study of structural, vibrational, and lattice dielectric properties of hafnium oxide. *Phys. Rev. B* **65**, 233106 (2002).
29 International Technology Roadmap for Semiconductors (2013) http://www.itrs.net/, accessed on May 2014.
30 Fulton, C. C., Cook, T. E. Jr., Lucovsky, G. & Nemanich, R. J. Interface instabilities and electronic properties of ZrO2 on silicon (100). *J. Appl. Phys.* **96**, 2665 (2004).
31 Snow, E. H., Grove, A. S., Deal, B. E. & Sah, C. T. Ion transport phenomena in insulating films. *J. Appl. Phys.* **36**, 1664 (1965).
32 Choi, B.-K. & Lockwood, D. J. Ionic conductivity and the phase transitions in Na_2SO_4. *Phys. Rev. B* **40**, 4683 (1989).
33 Moakafi, M., Khenata, R., Bouhemadou, A., Khachai, H., Amrani, B., Rached, D. & R'erat, M. Electronic and optical properties under pressure effect of alkali metal oxides. *Eur. Phys. J. B* **64**, 35–42 (2008).
34 Labat, F., Baranek, P., Domain, C., Minot, C. & Adamo, C. Density functional theory analysis of the structural and electronic properties of TiO_2 rutile and anatase polytypes: Performances of different exchange-correlation functionals. *J. Chem. Phys.* **126**, 154703 (2007).
35 Jaffe, J. E., Bachorz, R. A. & Gutowski, M. Low-temperature polymorphs of ZrO_2 and HfO_2: a density-functional theory study. *Phys. Rev. B* **72**, 144107 (2005).
36 Xiong, K., Robertson, J. & Clark, S. J. Behavior of hydrogen in wide band gap oxides. *J. App. Phys.* **102**, 083710 (2007).
37 Rignanese, G.-M. Dielectric properties of crystalline and amorphous transition metal oxides and silicates as potential high-κ candidates: the contribution of density-functional theory. *J. Phys. Condens. Matter* **17**, R357–R379 (2005).
38 Lukačević, I. High-pressure lattice dynamics and thermodynamics in BaO. *Phys. Status Solidi B* **248**, 1405–1411 (2011).
39 Lee, B., Lee, C.-K., Hwang, C.S. & Han, S. Influence of exchange-correlation functionals on dielectric properties of rutile TiO_2. *Curr. Appl. Phys.* **11**, S293–S296 (2011).

Supplementary Information accompanies the paper on the NPG Asia Materials website (http://www.nature.com/am)